Human Molecular Genetics, 2015, Vol. 24, No. 2 **525–539**
doi:10.1093/hmg/ddu472
Advance Access published on September 12, 2014

Identification and characterization of PKCγ, a kinase associated with SCA14, as an amyloidogenic protein

Hideyuki Takahashi[1,†], Naoko Adachi[1], Toshihiko Shirafuji[1], Sally Danno[1], Takehiko Ueyama[1], Michele Vendruscolo[2], Anton N. Shuvaev[3], Takuya Sugimoto[4], Takahiro Seki[5], Daizo Hamada[6], Kazuhiro Irie[4], Hirokazu Hirai[3], Norio Sakai[7] and Naoaki Saito[1,*]

[1]Biosignal Research Center, Kobe University, Kobe 657-8501, Japan, [2]Department of Chemistry, University of Cambridge, Lensfield Road, Cambridge CB2 1EW, UK, [3]Department of Neurophysiology, Gunma University Graduate School of Medicine, Maebashi, Gunma 371-8511, Japan, [4]Division of Food Science and Biotechnology, Graduate School of Agriculture, Kyoto University, Kyoto 606-8502, Japan, [5]Department of Chemico-Pharmacological Sciences, Graduate School of Pharmaceutical Sciences, Kumamoto University, Kumamoto 862-0973, Japan, [6]Department of Biochemistry and Molecular Biology, Graduate School of Medicine, Kobe University, Kobe 650-0017, Japan and [7]Department of Molecular and Pharmacological Neuroscience, Graduate School of Biomedical Science, Hiroshima University, Hiroshima 734-8551, Japan

Received June 12, 2014; Revised August 12, 2014; Accepted September 9, 2014

Amyloid assemblies are associated with a wide range of human disorders, including Alzheimer's and Parkinson's diseases. Here, we identify protein kinase C (PKC) γ, a serine/threonine kinase mutated in the neurodegenerative disease spinocerebellar ataxia type 14 (SCA14), as a novel amyloidogenic protein with no previously characterized amyloid-prone domains. We found that overexpression of PKCγ in cultured cells, as well as *in vitro* incubation of PKCγ without heat or chemical denaturants, causes amyloid-like fibril formation of this protein. We also observed that SCA14-associated mutations in PKCγ accelerate the amyloid-like fibril formation both in cultured cells and *in vitro*. We show that the C1A and kinase domains of PKCγ are involved in its soluble dimer and aggregate formation and that SCA14-associated mutations in the C1 domain cause its misfolding and aggregation. Furthermore, long-term time-lapse imaging indicates that aggregates of mutant PKCγ are highly toxic to neuronal cells. Based on these findings, we propose that PKCγ could form amyloid-like fibrils in physiological and/or pathophysiological conditions such as SCA14. More generally, our results provide novel insights into the mechanism of amyloid-like fibril formation by multi-domain proteins.

INTRODUCTION

Amyloid aggregates are associated with a great variety of human conditions including Alzheimer's and Parkinson's diseases. The term 'amyloid' was originally used for the extracellular unbranched fibrils that stain with histological dyes such as Congo red *in vivo*, including amyloid plaques in Alzheimer's disease. However, structurally similar 'amyloid-like' protein fibrils have also been found in many human neurodegenerative disorders such as cytoplasmic Lewy bodies in Parkinson's disease and intranuclear inclusions in polyglutamine diseases. Amyloid and amyloid-like fibrils, despite a lack of sequence and structural similarity in the native states of their component proteins, share common properties (1–4). Understanding the mechanism of formation of these aggregates is crucial to develop therapeutics for a wide range of amyloid-related diseases (5).

Protein kinase C (PKC) is a serine/threonine kinase of the AGC family that regulates intracellular signaling in numerous cellular processes (6,7). Among PKC isoforms, PKCγ is specifically expressed in the central nervous system and is especially abundant in cerebellar Purkinje cells (8,9). Mutations in PKCγ cause a dominantly inherited neurodegenerative disease,

*To whom correspondence should be addressed at: Biosignal Research Center, Kobe University, Kobe 657-8501, Japan. Email: naosaito@kobe-u.ac.jp
†Present address: Cellular Neuroscience, Neurodegeneration and Repair Program, Departments of Neurology and Neurobiology, Yale University School of Medicine, New Haven, CT 06536, USA.

spinocerebellar ataxia type 14 (SCA14) (10,11). PKCγ consists of an N-terminal regulatory and a C-terminal kinase domain. The regulatory domain of PKCγ contains two conserved domains, the diacylglycerol-binding C1 domain and the Ca^{2+}-binding C2 domain. The C1 domain is subdivided into the C1A and C1B domains having six conserved cysteines and two histidines in the typical core structure that coordinates two zinc ions. Accumulating evidence suggests that the C1A and C1B domains of PKC have distinct roles in its activation step and translocation (6,12). More than 30 mutations in PKCγ have been found in SCA14 patients, and most SCA14-associated mutations are found in the C1A and C1B domains of PKCγ, although several mutations in the C2 domain and the kinase domain of PKCγ have been also reported in SCA14 patients (13–18).

Previous studies have revealed that SCA14-associated mutant PKCγs form cytotoxic aggregates in the cytoplasm of primary cultured Purkinje cells as well as mammalian cell lines (19–23). Aggregates of mutant PKCγ have also been also found *in vivo* upon lentiviral expression in developing and mature mouse Purkinje cells (24). The amount of mutant PKCγ protein expressed in Purkinje cells was ∼23% of the endogenous PKCγ levels in this *in vivo* model, suggesting that mutant PKCγ could form aggregates in Purkinje cells in heterozygous SCA14 patients, where expression of mutant PKCγ should be ∼50% of the total amount of PKCγ (24). As it is generally believed that SCA14 is caused by a gain-of-function of mutant PKCγ, based on several lines of evidence including the data showing PKCγ knockout mice with no apparent atrophy in cerebellum, the aggregation of mutant PKCγ is thought to play a central role in the pathogenesis of SCA14 (13,25).

The aggregation mechanism of mutant PKCγ remains, however, unclear. In a screening for compounds that could affect aggregate formation of mutant PKCγ, we have recently found that Congo red is very effective in preventing aggregate formation of mutant PKCγ (26). As Congo red preferentially binds to β-sheets containing amyloid and amyloid-like fibrils to inhibit oligomerization (27,28), we hypothesized that mutant PKCγ aggregates might have characteristics of amyloid-like fibrils. Here, we show that mutant PKCγ indeed forms amyloid-like fibrils both *in vitro* and in cell culture models. Intriguingly, wild-type PKCγ was also shown to spontaneously form amyloid-like fibrils, suggesting that SCA14-associated mutations promote, but are not essential for, amyloid-like fibril formation. Mechanistically, native C1A and kinase domains were found to play a critical role in the amyloid-like fibril formation. Our findings thus provide novel insights into the pathogenesis of SCA14 as well as into the mechanism of amyloid fibril formation of multi-domain proteins.

RESULTS

Wild-type and mutant PKCγs form amyloid-like fibrils in cultured cells

The present study was prompted by the recent observation that Congo red is capable of inhibiting the aggregation of the SCA14-causing S119P mutant PKCγ (26). To build on this initial finding, we first examined whether Congo red also affects the aggregation of wild-type and other mutant PKCγ (Q127R and V138E) in cells. We utilized two cell lines, Chinese hamster ovary (CHO) cells and human neuroblastoma SH-SY5Y cells, in both of which mutant PKCγ has been shown to form aggregates with characteristics that are similar to those of aggregates in primary cultured Purkinje cells (20,22). We observed aggregates of PKCγ-green fluorescent protein (GFP) in ∼6% of SH-SY5Y cells overexpressing wild-type PKCγ-GFP, whereas overexpression of Q127R or V138E PKCγ-GFP increased the cells with the aggregates to ∼17%. Congo red treatment significantly reduced the aggregation of wild-type PKCγ-GFP, as well as Q127R and V138E PKCγ-GFP, in SH-SY5Y cells (Fig. 1A), suggesting that both wild-type and mutant PKCγ might form amyloid-like fibrils in cells. To further examine whether PKCγ forms amyloid-like fibrils, we performed thioflavin S staining for aggregates of mutant PKCγ tagged with DsRed-monomer (PKCγ-DRm). Thioflavin S fluorescence was partially co-localized with perinuclear aggregates of mutant PKCγ-DRm in CHO cells (Fig. 1B), whereas it was hardly detected in the perinuclear region of non-transfected CHO cells (Supplementary Material, Fig. S1). Furthermore, using electron microscopy (EM), we observed a great number of fibrils in the perinuclear aggregates of both wild-type and mutant (S119P and G128D) PKCγ in CHO cells (Fig. 1C–H). Taken together, these results indicate that overexpression of wild-type PKCγ is sufficient to form amyloid-like aggregates in cells and that SCA14-associated mutations promote amyloid-like fibril formation.

Mutant PKCγ spontaneously forms amyloid-like fibrils *in vitro*

We next sought to examine whether the recombinant mutant PKCγ forms amyloid-like fibrils *in vitro*. We purified and utilized glutathione-S-transferase (GST)-tagged full-length Q127R and V138E PKCγ (Fig. 2A). Western blot analysis revealed that after 24 h of incubation at 37°C, recombinant mutant PKCγ formed a high-molecular-weight (MW) oligomeric species (>250 kDa). In addition, further incubation (48–72 h) of mutant PKCγ yielded SDS-insoluble, high-MW aggregates that did not enter the stacking gel (Fig. 2B). A concomitant decrease of monomeric forms was also detected, suggesting that high-MW aggregates are mainly formed from monomeric PKCγ, possibly via high-MW oligomers. Glutathione-S-transferase alone did not show any high-MW aggregates after 72 h of incubation (Supplementary Material, Fig. S2). These high-MW aggregates have frequently been observed in other disease-causing proteins, such as polyglutamine-expanded huntingtin in Huntington's disease that forms amyloid-like fibrils (29). When mutant PKCγ was observed after 3–10 days of incubation under EM, a number of amorphous aggregates (Fig. 2C) and several long straight filaments (Fig. 2D–G) were found. Some fibrils appeared to grow from amorphous aggregates (Fig. 2E). Interestingly, some of the fibrils appeared to exhibit a twisted two-filament architecture (Fig. 2F) reminiscent of amyloid β fibrils formed *in vitro* (30). We also performed a thioflavin T (ThT) binding assay. Thioflavin T binds to β sheets in amyloid oligomers, producing a characteristic fluorescent emission at 482 nm (31). Thioflavin T fluorescence

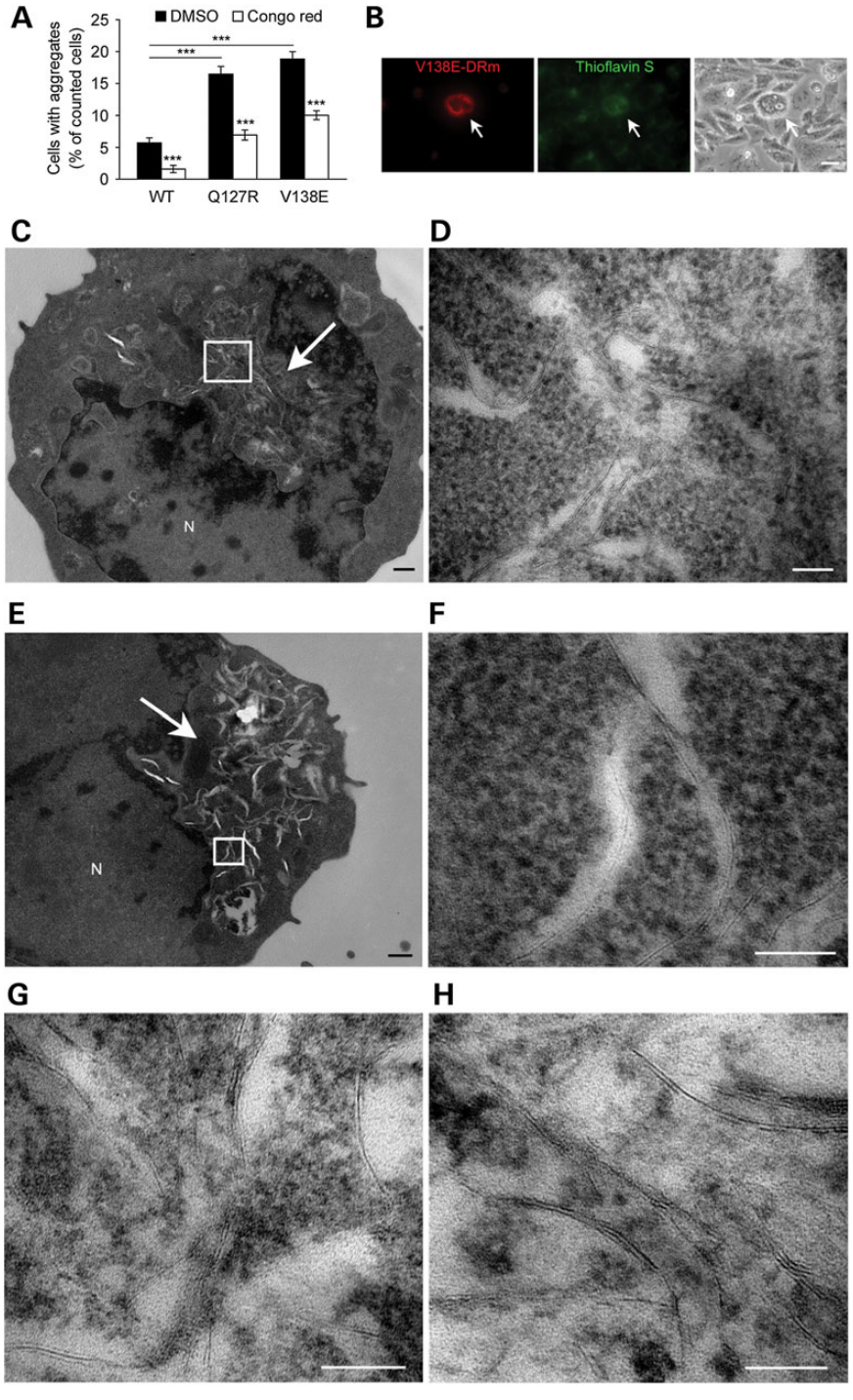

Figure 1. Wild-type and mutant PKCγs form amyloid-like fibrils in cells. (**A**) Effects of Congo red on the aggregation of mutant PKCγ-GFP in cells. SH-SY5Y cells transfected with wild-type, Q127R and V138E PKCγ-GFPs were treated with 100 μM Congo red 4 h after transfection. One day after transfection, the fixed cells were counted. Data are shown as mean ± SEM ($n = 3$). $^{***}P < 0.001$ (ANOVA, Tukey's test). (**B**) CHO cells expressing V138E PKCγ-DRm were stained with thioflavin S. Arrows indicate cells expressing V138E PKCγ-DRm. The bar is scaled to 20 μm. (**C**) A CHO cell expressing G128D PKCγ-GFP was observed under EM. N indicates the nucleus. The arrow indicates perinuclear aggregates. The bar is scaled to 500 nm. (**D**) An image of the rectangular area in (C) is magnified. The bar is scaled to 100 nm. (**E**) A CHO cell expressing S119P PKCγ-GFP was observed under EM. N indicates the nucleus. The arrow indicates perinuclear aggregates. The bar is scaled to 500 nm. (**F**) An image of the rectangular area in (E) is magnified. The bar is scaled to 100 nm. (**G**) Perinuclear aggregates of a CHO cell expressing S119P PKCγ-GFP were observed under EM. The bar is scaled to 100 nm. (**H**) Perinuclear aggregates of a CHO cell expressing wild-type PKCγ-GFP were observed under EM. The bar is scaled to 100 nm.

increased over time (Fig. 2H), a characteristic of amyloids. Thioflavin T fluorescence also started to decline after 8 days, indicating the formation of large fibers that do not bind efficiently to ThT. We also found that the treatment with Congo red reduces high-MW aggregate formation of recombinant V138E PKCγ (Fig. 2I). Thus, these results clearly showed that recombinant mutant

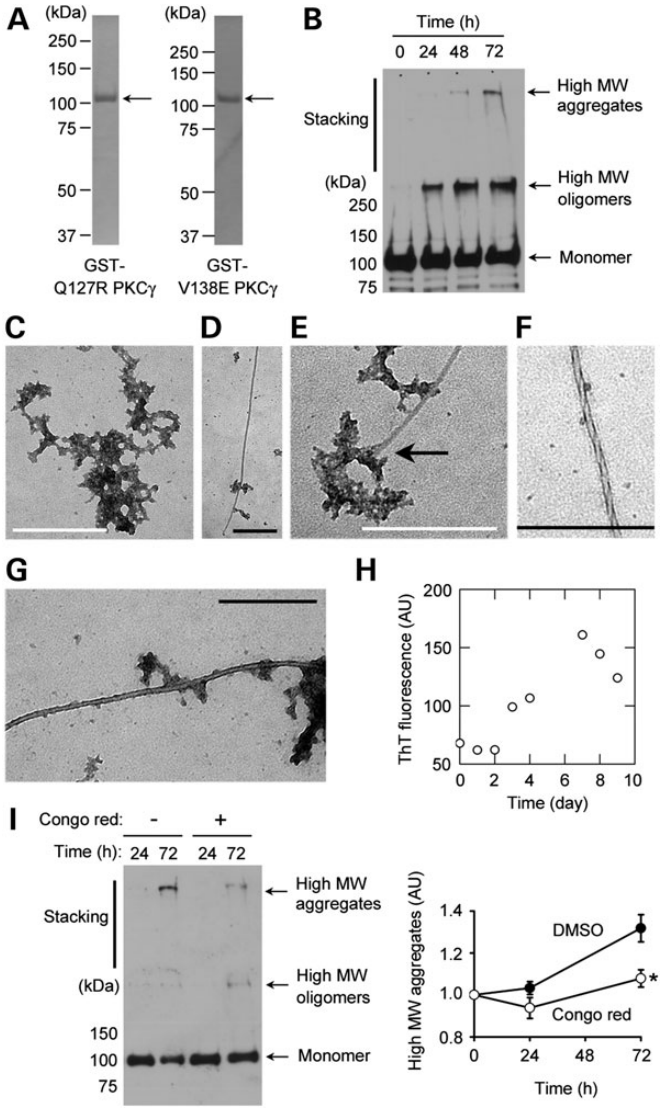

Figure 2. Mutant PKCγ spontaneously forms amyloid-like fibrils *in vitro*. (**A**) Coomassie Brilliant Blue staining of the purified recombinant GST-tagged Q127R and V138E PKCγ. Arrows indicate the recombinant proteins. (**B**) Purified recombinant GST-tagged Q127R PKCγ was incubated at 37°C for the indicated amount of time and subjected to SDS–PAGE and immunoblotting with anti-PKCγ antibodies. (**C**–**F**) Purified recombinant GST-tagged Q127R PKCγ was incubated at 37°C for 3 days and subsequently observed by EM. The arrow indicates a filament grown from amorphous aggregates. The bar is scaled to 500 nm. (**G**) Purified recombinant GST-tagged V138E PKCγ was incubated at 37°C for 10 days and subsequently observed by EM. The bar is scaled to 500 nm. (**H**) Thioflavin T fluorescence of GST-tagged V138E PKCγ (35 μg/ml). (**I**) Purified recombinant GST-tagged V138E PKCγ was incubated at 37°C with or without 100 μM Congo red for the indicated amount of time and subjected to SDS–PAGE and immunoblotting with anti-PKCγ antibodies. Data are shown as mean ± SEM ($n = 3$). $^*P < 0.05$ (unpaired Student's *t*-test).

PKCγ spontaneously forms aggregates *in vitro* with characteristic amyloid features.

Wild-type PKCγ also forms amyloid-like fibrils *in vitro*

We also considered whether recombinant GST-tagged wild-type PKCγ forms amyloid-like fibrils *in vitro*. Similar high-MW aggregates were also consistently detected 72 h after incubation of wild-type PKCγ (Fig. 3A and B). Electron microscopy analysis also showed several long straight twisted fibrils in the incubated sample of GST-tagged wild-type PKCγ (Fig. 3C). These data indicate that wild-type PKCγ also spontaneously forms amyloid-like fibrils and that SCA14-associated mutations are not essential for amyloid-like aggregation *in vitro*. To examine whether SCA14-associated mutations affect the amyloid-like fibril formation, we performed the ThT binding assay using lower concentrations of recombinant wild-type and Q127R PKCγs. Under these conditions, ThT fluorescence was only slightly increased in wild-type PKCγ, whereas there was an increase in the ThT fluorescence in Q127R PKCγ, suggesting that a SCA14-associated mutation promotes amyloid-like fibril formation of PKCγ *in vitro* (Fig. 3D). To further examine whether endogenous wild-type PKCγ could form aggregates *in vivo*, we performed western blot analysis using the TBS-soluble, the Triton-soluble and the Triton-insoluble fractions of the mouse cerebellum. Anti-PKCγ antibodies detected an immunoreactive monomer band in the Triton-insoluble fraction. In addition, similar to our *in vitro* data, high-MW aggregates band was detected in the total and the Triton-insoluble fractions. Interestingly, we also detected high-MW oligomers band (~250 kDa) in all fractions except the Triton-insoluble fraction (Fig. 3E). These results suggest the possibility that endogenous wild-type PKCγ could form amyloid-like aggregates *in vivo*.

Prediction of aggregation-prone regions in PKCγ

We next sought to understand the mechanisms whereby wild-type and mutant PKCγ forms amyloid-like fibrils. As PKCγ has no previously characterized amyloid-prone domains, we first utilized the Zyggregator method, which predicts the regions that promote the aggregation of structured globular proteins or proteins that contain both structured and unstructured domains (32). The method revealed that wild-type PKCγ has many potential aggregation-prone regions (Fig. 4). The aggregation-prone regions were relatively concentrated in the C1A, the C1B and the kinase domains, which seemed to be correlated with the locations of SCA14-associated mutations (Fig. 4). These predictions also suggest that native C1A, C1B and kinase domains of PKCγ might play a critical role in the amyloid-like fibril formation of both wild-type and mutant PKCγ.

The C1A and kinase domains are involved in soluble dimerization and aggregation of mutant PKCγ

Based on the prediction described earlier, we hypothesized that the C1A, the C1B or the kinase domain may also play a critical role in the aggregate formation of PKCγ. To test the idea, we focused on V138E PKCγ, a mutant PKCγ with a mutation in the C1B domain, because most SCA14-associated mutations are found in the C1B domain. We first performed co-transfection studies using V138E PKCγ-DRm and each of the GFP-tagged domains: GFP-tagged C1A, C1B, C2 or kinase domains (C1A-GFP, C1B-GFP, C2-GFP or KD-GFP, respectively). We found that C1A- and KD-GFP, but not C1B- and C2-GFP, were significantly incorporated into the aggregates of V138E PKCγ-DRm (Fig. 5A). Consistent with these results, wild-type PKCγ-GFP is also incorporated with V138E PKCγ-DRm

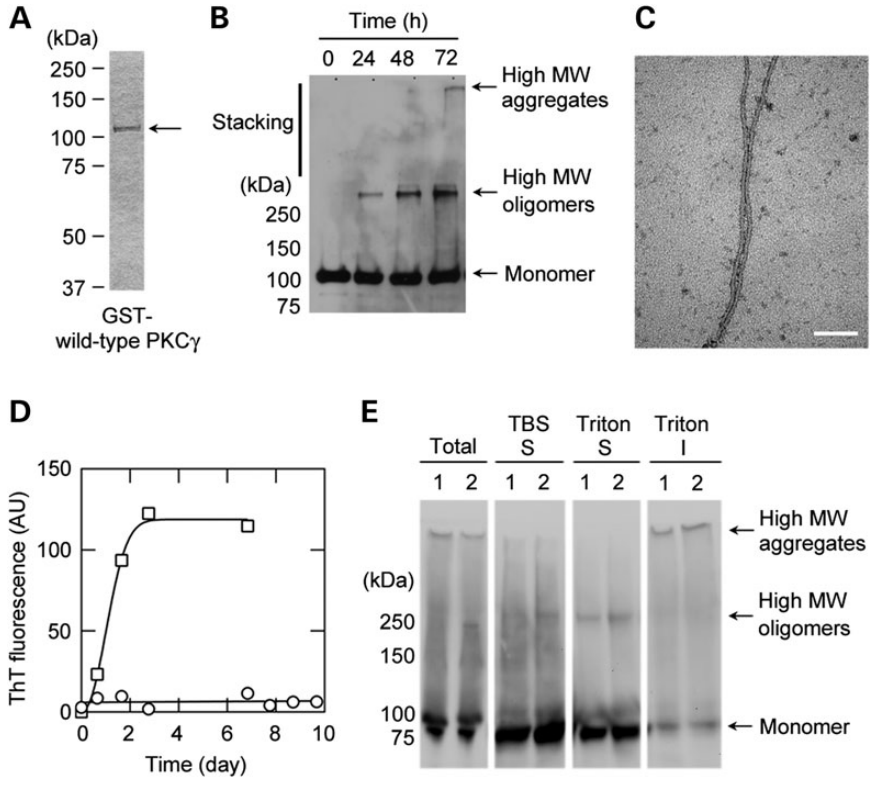

Figure 3. Wild-type PKCγ also forms amyloid-like fibrils *in vitro*. (**A**) Coomassie Brilliant Blue staining of the purified recombinant GST-tagged wild-type PKCγ. The arrow indicates the recombinant protein. (**B**) Purified recombinant GST-tagged wild-type PKCγ was incubated at 37°C for the indicated amount of time and subjected to SDS–PAGE and immunoblotting with anti-PKCγ antibodies. (**C**) Purified recombinant GST-tagged wild-type PKCγ was incubated at 37°C for 3 days and subsequently observed by EM. The bar is scaled to 100 nm. (**D**) Thioflavin T fluorescence of GST-tagged wild-type (open circle) and Q127R PKCγ (open square) (10 μg/ml). (**E**) The TBS-soluble, the Triton-soluble and the Triton-insoluble fractions of the mouse cerebellum were subjected to SDS–PAGE and immunoblotting with anti-PKCγ antibodies. The numbers indicate two individual mice. S and I indicate soluble and insoluble, respectively. Data are representative from experiments using three mice with similar results.

aggregates. Similar results from reversed experiments using V138E PKCγ-GFP and each DRm-tagged domain excluded the possibility that DRm was sticky and had an affinity toward C1A- and KD-GFP (Supplementary Material, Fig. S3A). These findings suggest that intact C1A and kinase domain may be involved in aggregate formation of mutant PKCγ, even in PKCγ with a C1B domain mutation.

As soluble dimers and/or oligomers are formed before insoluble aggregates in most neurodegenerative-associated proteins (33,34), we examined whether mutant PKCγ forms soluble dimers and/or oligomers. To this end, we performed co-immunoprecipitation (co-IP) assays with a Triton-soluble fraction of COS-7 cells. The co-IP assays with full-length PKCγ showed self-association of wild-type PKCγ. In addition, we found that SCA14–associated mutations dramatically promote self-association of full-length PKCγ (Fig. 5B and Supplementary Material, Fig. S3B). The co-IP assays using domains from PKCγ revealed three possible self-association regions, specifically C1A–C1A domains, C1A–kinase domains and kinase–kinase domains interactions (Supplementary Material, Fig. S4A–D). The C1A and the kinase domain, but not the C1B or the C2 domain, also interacted with full-length V138E PKCγ (Fig. 5C). These results suggest that the C1A and the kinase domains of mutant PKCγ with a C1B domain mutation are involved in the soluble dimer formation that eventually leads to its aggregation. The co-IP assays using mutated domains showed that mutations in C1B (V138E), C1A (R41P) and kinase domain (F643L) could not alter its interaction partners (Supplementary Material, Fig. S4E–G).

SCA14-associated mutations impair the [^{3}H]phorbol 12,13-dibutyrate-binding ability of the C1A or C1B domain of PKCγ

We next sought to gain insight into the effects of SCA14-associated mutations on aggregate formation. We focused on the C1 domain of PKCγ, because most SCA14-associated mutations of PKCγ are located within C1A and C1B that bind to membrane diacylglycerol or tumor-promoting phorbol esters (Figs. 4 and 6A). To examine whether SCA14-associated mutations affect the function and folding of the C1 domain, we performed an *in vitro* [^{3}H]phorbol 12,13-dibutyrate (PDBu)-binding assay using wild-type and mutated C1A and C1B peptides as previously reported (35). We did not examine the C1 domains with mutations at cysteine residues, such as C114Y and C131R, because these mutations were assumed to cause the complete loss of PDBu-binding ability by causing their inability to coordinate zinc, as reported in a previous study (36). Consistent with a previous study, the K_d values of wild-type C1A and C1B peptide were 1.36 and 1.2 $\pm$ 0.06 nM, respectively (35). In contrast, the K_d values of mutated C1A and C1B peptides were significantly higher. In addition, several mutated

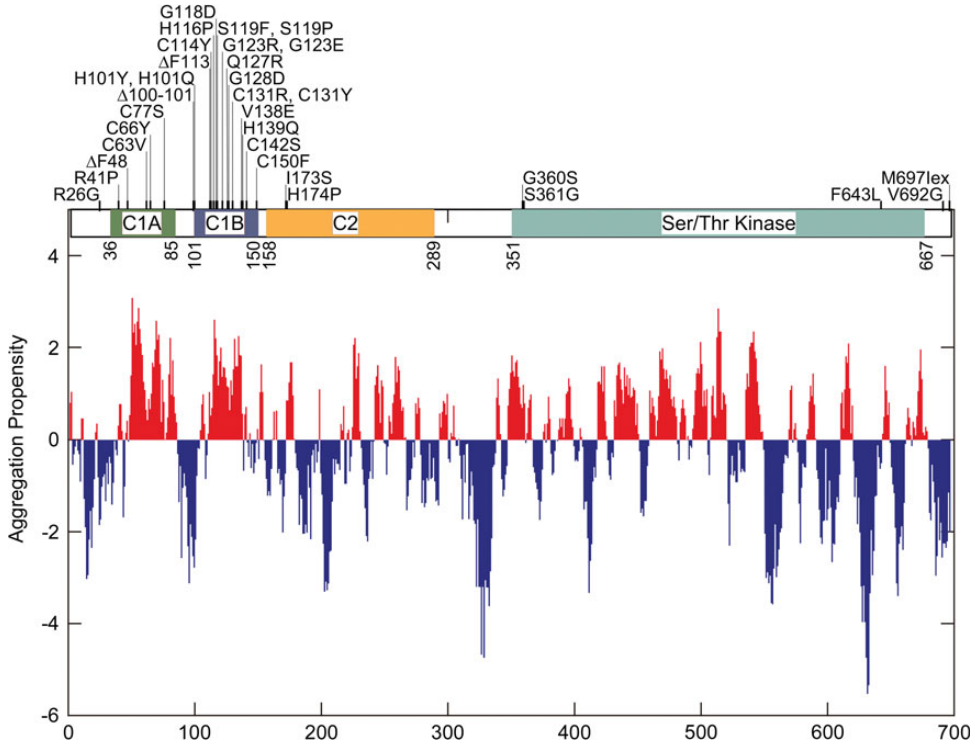

Figure 4. The prediction of aggregation-prone regions of PKCγ. The aggregation propensity of wild-type PKCγ was calculated with the Zyggregator method. The positive and negative scales mean higher and lower aggregation propensity, respectively. The locations of the SCA14-associated mutations and domains of PKCγ are also shown in the data.

C1A or C1B peptides (R41P, G63V, Q127R and G128D) showed no PDBu-binding ability (Table 1). Notably, none of SCA14-associated mutations we tested increased the PDBu-binding ability of the C1 domain. These results indicate that SCA14-associated mutations impair the PDBu-binding ability of the C1A or C1B domain of PKCγ and suggest that the mutations in the C1 domain might cause its misfolding.

SCA14-associated mutations in C1 domain cause its aggregation in cells

To determine whether the mutations in C1 domain cause its misfolding, we examined whether mutated C1A, C1B or whole C1 domain alone forms aggregates using CHO cells expressing C1A-, C1B- or C1-GFP. Compared with wild-type C1A-GFP and C1B-GFP, all tested mutated C1A-GFP (R41P and G63V C1A-GFP) and C1B-GFPs (H101Y, C114Y, S119P and V138E C1B-GFP) except Q127R C1B-GFP tended to form aggregates in the perinuclear region of CHO cells (Fig. 6B and C), although their size was relatively smaller than the full-length mutant protein aggregates previously reported (19). Moreover, GFP-tagged mutated whole C1 domains also formed perinuclear aggregates (Fig. 6D). These data support the possibility that the mutations in C1 domain cause its misfolding and also suggest that mutated C1 domain may be directly involved in the aggregate formation of mutant PKCγ.

Aggregation of mutant PKCγ is highly cytotoxic

We next sought to understand the relationship between mutant PKCγ aggregation and cytotoxicity. We performed long-term time-lapse imaging of living SH-SY5Y cells expressing mutant PKCγ-GFP with the LCV-100 or LCV-110 incubation imaging system, which enables to monitor several individual cells transfected with several distinct plasmids as well as the same plasmid over time at the same time in an independent experiment. Four mutants (R41P, H101Y, Q127R and F643L) were selected to determine whether mutant PKCγ can form toxic aggregates, regardless of the location of the mutation (i.e. the C1A, the C1B or the kinase domain). These mutations were selected because they have also been found in a relatively large number of SCA14 patients (37–39). Individual cells transfected with these four mutant PKCγ-GFPs were monitored 1 day after transfection for 22 h. Similar to previous studies with CHO cells and primary cultured Purkinje cells (20,22), it was observed that several cells, in which no visible aggregates were initially detected, formed cytoplasmic aggregates of mutant PKCγ-GFP. The formation of these aggregates was followed by shrinkage, an early apoptotic-like morphological change (40), and complete detachment from the cultured dish (Fig. 7A and Supplementary Material, Movie S1). We first examined the survival time of all cells that died within the observation period after aggregate formation of mutant PKCγ-GFPs. Cell death was defined as irreversible detachment from the cultured dish after shrinkage because we have previously observed caspase activation as well as ubiquitin-proteasome system impairment and ER stress in cells that exhibit this type of behavior (20). Surprisingly, more than 80% of cell deaths with visible mutant PKCγ aggregates were caused within 10 h after aggregate formation. In addition, similar results were obtained with four different mutant PKCγ-GFPs (Fig. 7B and

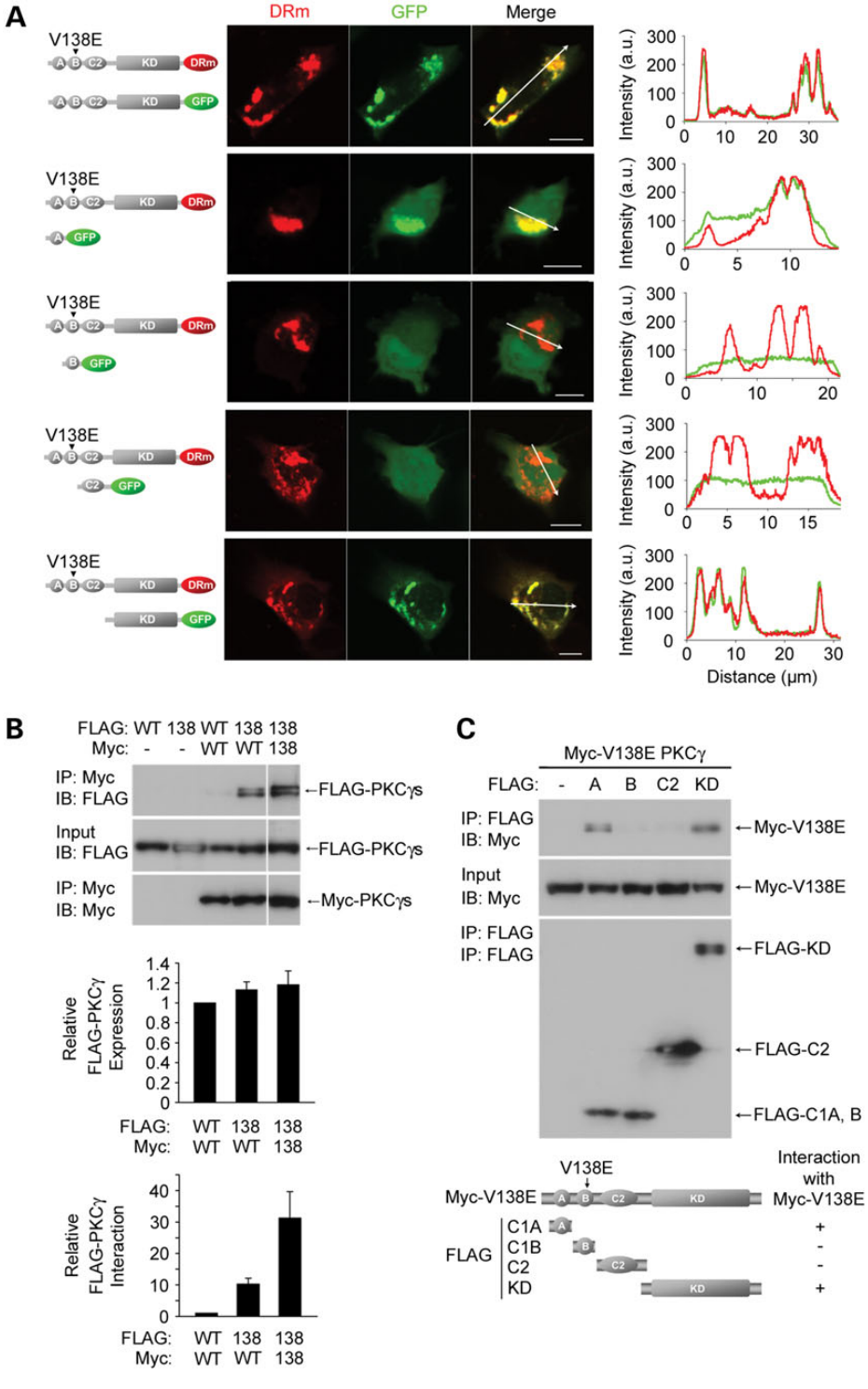

Figure 5. The C1A and kinase domains are involved in soluble dimerization and aggregation of mutant PKCγ. (**A**) C1A domain (C1A) and kinase domain (KD) are incorporated into the mutant PKCγ aggregates. SH-SY5Y cells co-transfected with GFP-tagged wild-type PKCγ or constructs in each domain (C1A, C1B, C2 or KD) and V138E PKCγ-DRm were observed by confocal microscopy. Graphs depict fluorescent intensity of the two channels along the white arrows indicated on the merge images. The bar is scaled to 10 μm. (**B**) SCA14-associated mutations promote self-association of PKCγ in the soluble fraction. COS-7 cells were co-transfected with FLAG- and Myc-wild-type or V138E PKCγ. The cell lysates were immunoprecipitated (IP) with anti-Myc antibodies and subsequently immunoblotted (IB) with anti-Myc or anti-FLAG antibodies. The middle bar graph represents the quantification of FLAG-PKCγ expression. The bottom bar graph represents the quantification of FLAG-PKCγ interactions (co-immunoprecipitated FLAG-PKCγ) normalized to the amount of immunoprecipitated Myc-PKCγ. Data are shown as mean ± SEM ($n = 3$). (**C**) C1A and KD interact with mutant PKCγ in the soluble fraction. COS-7 cells were co-transfected with FLAG-C1A, C1B, C2 or KD along with Myc-V138E PKCγ. The cell lysates were immunoprecipitated (IP) with anti-FLAG antibodies and subsequently immunoblotted (IB) with anti-Myc or anti-FLAG antibodies. This experiment was replicated three times with similar results.

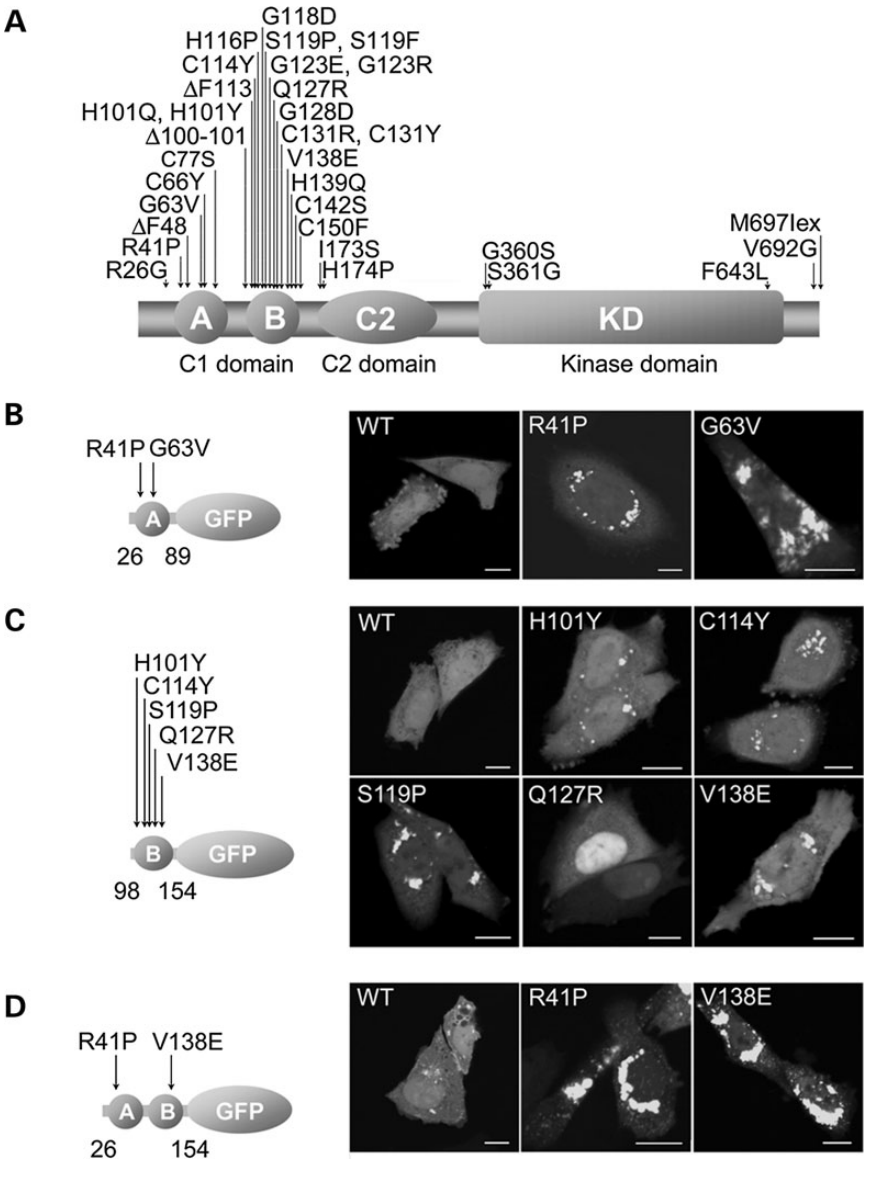

Figure 6. SCA14-associated mutations in the C1 domain cause its aggregation in cells. (**A**) Scheme of PKCγ domains and SCA14-associated mutations in PKCγ. PKCγ has an N-terminal regulatory domain and a C-terminal kinase domain. The regulatory domain contains a diacylglycerol-sensitive, cysteine-rich C1 domain (C1A and C1B) and a Ca^{2+}-binding C2 domain. Arrows indicate the locations of the SCA14-associated mutations. M697Iex indicates a missense change (M697I) and a C-terminal 13-amino-acid extension by a deletion that includes a stop codon. (**B**) CHO cells transfected with GFP-tagged wild-type, R41P or G63V C1A domain were observed by confocal microscopy. The bar is scaled to 10 μm. (**C**) CHO cells transfected with GFP-tagged wild-type, H101Y, C114Y, S119P, Q127R or V138E C1B domain were observed by confocal microscopy. The bar is scaled to 10 μm. (**D**) CHO cells transfected with GFP-tagged wild-type, R41P or V138E C1 domain were observed by confocal microscopy. The bar is scaled to 10 μm.

Supplementary Material, Movies S2–S4). We subsequently examined the lifespan of individual cells, with or without visible aggregates 1 day after transfection, and determined the level of difference using survival analysis for 10 h, as previously reported (41). The survival analysis showed that in the four different mutant PKCγ-GFPs-expressing cells, cells with visible mutant PKCγ-GFP aggregates died faster than cells without aggregates (Fig. 7C–F). These results indicate that aggregate formation of at least four different mutant PKCγs is highly cytotoxic.

We also examined the relationship between cytotoxicity and fluorescent intensity of diffuse mutant PKCγ-GFP. The survival time of individual cells with diffuse mutant PKCγ-GFP was not correlated with their maximum GFP fluorescent intensity on the first day after transfection in all of four of the different mutant PKCγ-GFPs (Fig. 7C–F, Inset). We further examined the lifespan of individual cells expressing diffuse wild-type PKCγ-GFP, Q127R PKCγ-GFP or non-fused GFP in another set of four independent experiments. Diffuse Q127R PKCγ-GFP was equally as cytotoxic as diffuse wild-type PKCγ-GFP, whereas diffuse non-fused GFP was significantly less cytotoxic (Fig. 7G and H). Similar results were obtained with cells expressing wild-type and Q127R PKCγ fused to the C-terminus of mCherry (Supplementary Material, Fig. S5A–C), excluding

Table 1. PDBu binding of wild-type or mutant PKCγ C1 peptides.

Peptide	K_d (nM)	B_{max} (%)
Wild-type-C1A	1.36	38.6
R41P-C1A	No binding	
G63V-C1A	No binding	
Wild-type-C1B	1.2 ± 00.6	35.5 ± 1.7
H101Y-C1B	44.3 ± 6.5	2.9 ± 0.3
S119P-C1B	14.0 ± 0.08	4.8 ± 1.2
Q127R-C1B	No binding	
G128D-C1B	No binding	
V138E-C1B	82.1 ± 0.5	15.2 ± 1.3

Results are means ± s.e.m. for at least two separate experiments, except that of PDBu binding of wild-type C1A.

the possibility that the cytotoxic effects of mutant PKCγ are specific to mutant PKCγ fused to the N-terminus of GFP. These results revealed that the aggregation process plays a role in the cytotoxic effects of mutant PKCγ.

DISCUSSION

In this study, we identified PKCγ, a kinase associated with spinocerebellar ataxia, as a novel amyloidogenic protein with no previously characterized amyloid-prone domains.

The mechanisms of amyloid-like fibril formation of PKCγ

Our results indicate that the C1A and kinase domains are involved in the soluble dimer and aggregate formation of wild-type and mutant PKCγ with C1B mutation. The co-IP assay also showed that C1A–C1A, C1A–kinase and kinase–kinase domains interactions may represent the common inter-molecular interaction sites of mutant PKCγ. It is possible that the C1A–kinase domains interaction is also an intra-molecular interaction site of PKCγ, although a recently published crystal structure of full-length PKCβII isoform showed only the C1B–kinase domains interaction (42). Three-dimensional structures of full-length PKCγ are yet to become available. Access to these structures would help understand the conformation and aggregation process of wild-type and mutant PKCγ. It is well known that the C1 domains are highly hydrophobic and involved in protein–protein interactions as well as lipid–protein interactions (12). The kinase domain also contains several hydrophobic regions (6). These hydrophobic regions therefore may mediate the dimerization and aggregation of PKCγ.

In this study, we have shown that SCA14-associated mutations promote the amyloid-like fibril formation of PKCγ both in cells and *in vitro*. There are several possible explanations about how SCA14-associated mutations enhance aggregation. Our results indicate that several SCA14-associated mutations in C1 domain impair its phorbol ester binding, suggesting that mutations in the C1 domain cause improper folding, probably by diminishing zinc coordination and/or perturbing the stability of the secondary and tertiary structures. Mutated C1A or C1B domains alone were also shown to form small aggregates in CHO cells. Therefore, first, mutated C1 domain may directly contribute to the aggregate formation of mutant PKCγ, as described later. Second, the mutations in the C1 domain might cause cytoplasmic accumulation of PKCγ by impairing its membrane diacylglycerol binding. Third, most importantly, the improper folding of the C1 domain may destabilize the inactive (closed) conformation of full-length PKCγ, which may enhance inter-molecular interactions and amyloid-like fibril formation. This idea is supported by previous studies showing that most mutant PKCγ-GFPs are constitutively active (23,43,44). Verbeek and colleagues have also suggested that SCA14 mutations in C1B 'open' PKCγ protein conformation (45). SCA14-associated mutations in the kinase domain (G360S, S361G and F643L) also increase aggregate formation of PKCγ (13,19). We have shown that these kinase domain mutations increase the formation of soluble dimers. As a previous study has suggested that kinase domain mutations in PKCλ may affect the overall conformation of the protein (46), the kinase domain mutations in PKCγ may also destabilize the closed conformation by disrupting intra-molecular interactions and promote inter-molecular interactions.

Taken together, we propose the following mechanisms whereby wild-type and mutant PKCγ (mainly for C1B mutations) forms amyloid-like fibrils (Fig. 8). SCA14-associated mutations may affect native folding of C1B domain to cause cytosolic accumulation and to destabilize closed conformation of PKCγ, which may expose buried inside regions of C1A and kinase domains of mutant PKCγ. Newly exposed regions of C1A and kinase domains in turn cause aberrant inter-molecular interaction of mutant PKCγ via C1A–C1A domains, C1A–kinase domains and kinase–kinase domains interactions. These inter-molecular interactions may promote oligomerization, aggregation and amyloid-like fibril formation of mutant PKCγ. This model for amyloid-like fibril formation may be, at least in part, supported by previously published 'Gain-of-interaction models', where a 3D domain swapping like C1A–kinase domains interaction has been suggested (47). We have shown that mutated C1B-GFP forms aggregates in cells, suggesting that mutated C1B alone has an ability to directly form cross-β spine and amyloid-like fibrils. Recently, in Huntington's disease, N-terminal 17 amino acids of huntingtin were shown to promote polyglutamine expansions to form amyloid (48,49). Similarly, C1A and kinase domains might support and promote mutated C1B domain to form cross-β spine. While most mutated C1B domains formed aggregates, we did not observe aggregates of the C1B domain with the Q127R mutation despite robust aggregation of full-length Q127R PKCγ in cells. These results suggest that the mechanism of aggregate formation of full-length Q127R PKCγ may be different from other C1B mutants and that the aggregation of full-length Q127R PKCγ may not require the C1B domain aggregation caused by its misfolding. In addition, the results also suggest that the inter-molecular interactions, rather than mutated C1B domain aggregation, might play a critical role in aggregate formation of full-length mutant PKCγ. With regard to wild-type PKCγ, repetitive physiological stimuli may destabilize the closed conformation, which could lead to inter-molecular interactions and aggregation of wild-type PKCγ.

The relationship between PKCγ aggregates and cytotoxicity

It is still under debate whether amyloid or amyloid-like aggregates are pathogenic, incidental or protective in many neurodegenerative diseases (50). Recently, soluble oligomers, rather than larger

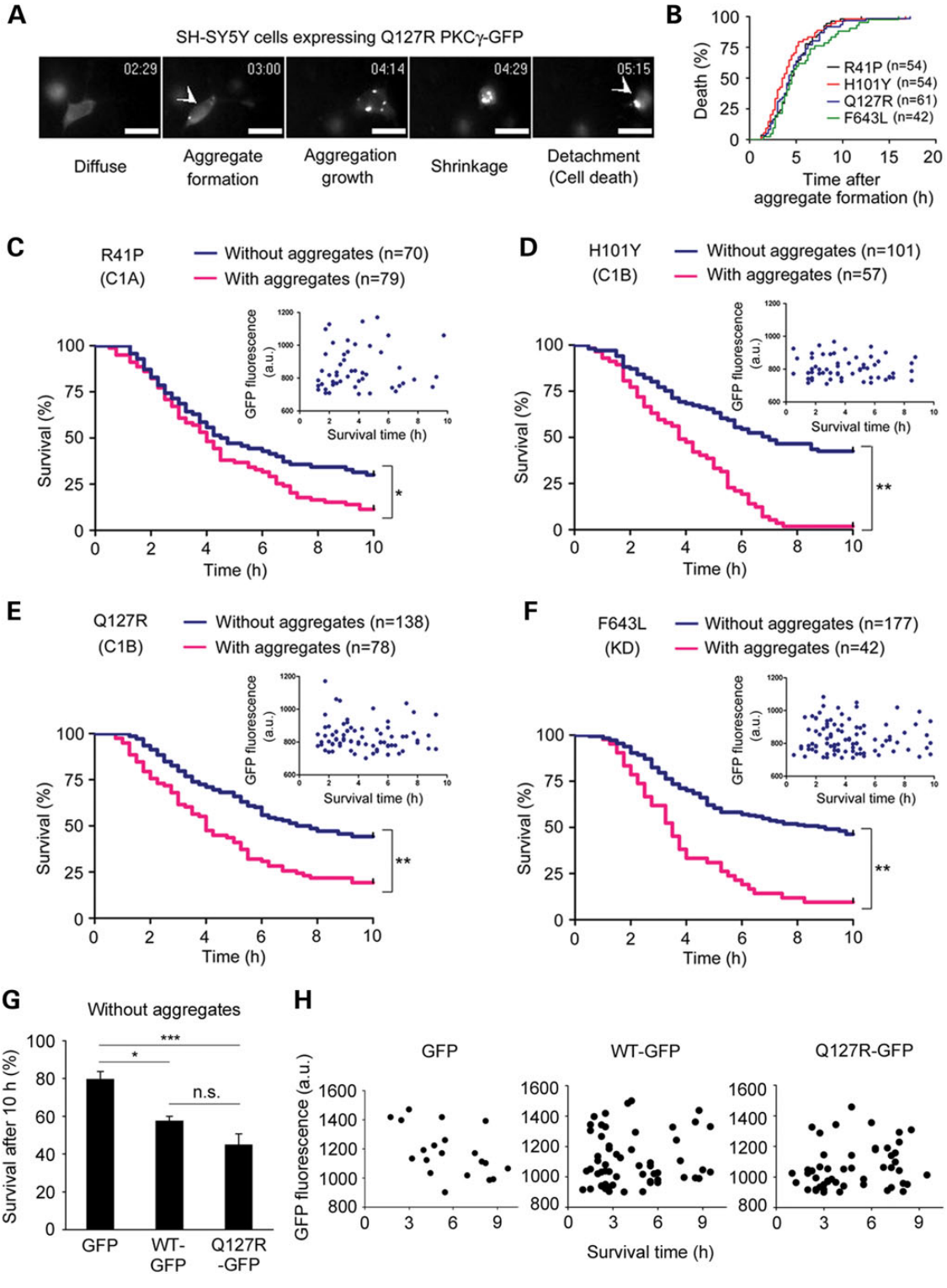

Figure 7. Aggregation process of mutant PKCγ is highly cytotoxic. (**A**–**F**) SH-SY5Y cells transfected with four mutant PKCγ-GFPs (R41P, H101Y, Q127R or F643L) were observed using an incubation imaging system. Pictures were taken every 15 min, and the data were analyzed using MetaMorph software, as described in Materials and Methods. The representative videos are available in the Supplementary Material, Movies S1, S2, S3 and S4. All data were obtained from seven independent experiments. (**A**) Sequential fluorescent images of an SH-SY5Y cell expressing Q127R PKCγ-GFP and definition of aggregate formation (first arrowhead) and cell death (second arrowhead). The bar is scaled to 20 μm. (**B**) Cumulative percentages of cell death after mutant PKCγ aggregate formation. We were able to evaluate 7.7 ± 3.9, 7.7 ± 4.5, 8.6 ± 1.7 and 6.0 ± 4.2 (mean ± SD) cells with aggregates of mutant PKCγ (R41P, H101Y, Q127R and F643L, respectively) which were evaluated in each experiment. (**C**–**F**) Kaplan–Meier survival curve showing the reduced lifespan of aggregate-containing cells 10 h after observation. We were able to evaluate 11.2 ± 4.3, 8.1 ± 3.3, 11.1 ± 3.8 and 6.0 ± 2.6 (mean ± SD) cells with aggregates of mutant PKCγ (R41P, H101Y, Q127R and F643L, respectively) in each experiment. We evaluated all cells with diffuse mutant PKCγ with a maximum fluorescent intensity of >700 in each experiment. We were able to evaluate

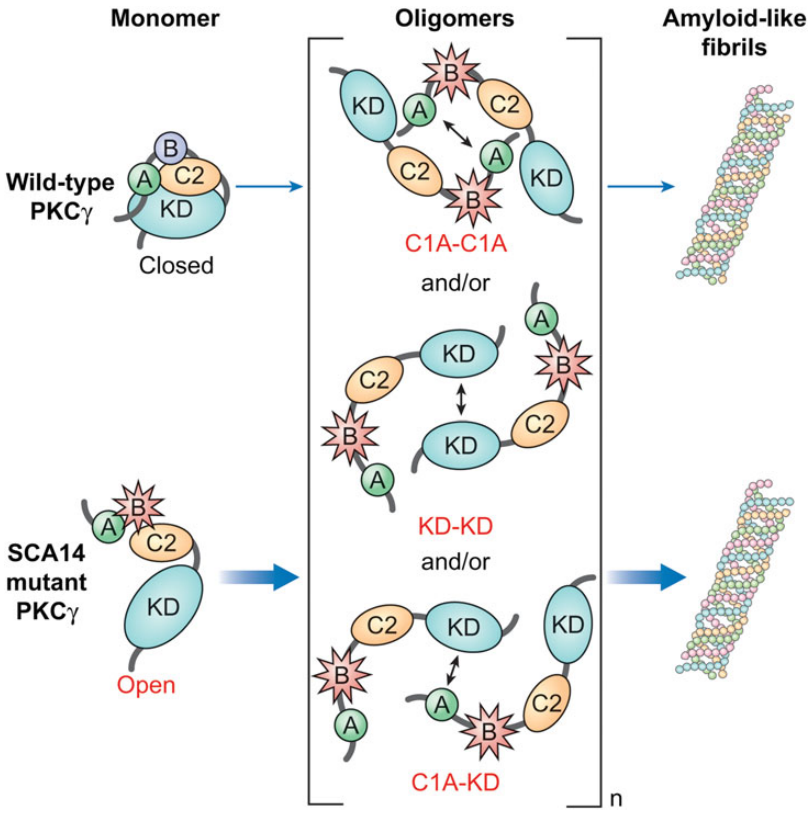

Figure 8. Hypothetical model of amyloid-like fibril formation of PKCγ. SCA14-associated mutations in the C1 (C1A or C1B) domain may cause improper folding by diminishing zinc coordination and/or perturbing the secondary and tertiary structure. The improper folding of the C1 domain may destabilize the closed conformation of PKCγ. In cells, the impaired membrane-binding ability of the C1 domain may also cause cytoplasmic accumulation of PKCγ. The destabilized PKCγ may expose buried inside regions of its C1A and kinase domains. Then, newly exposed regions of the C1A and kinase domains in turn cause aberrant inter-molecular interaction of PKCγ via C1A–C1A domains, C1A–kinase domains and kinase–kinase domains interactions. These interactions may promote oligomerization, aggregation and amyloid-like fibril formation of mutant PKCγ. Other factors such as PKCγ-interacting proteins may also affect self-association of PKCγ in cells.

aggregates, have been proposed as the agents responsible for neurodegeneration (33,34). We have previously demonstrated that aggregate formation of S119P and G128D mutant PKCγ impairs the ubiquitin-proteasome system and induces endoplasmic reticulum stress in cultured Purkinje cells, leading to apoptotic cell death (20,22). In the current study, using long-term time-lapse imaging analysis, we have confirmed and expanded our previous studies. It was directly demonstrated that regardless of the location of the mutation (R41P, H101Y, Q127R or F643L), the aggregation of mutant PKCγ is highly cytotoxic. We have also observed early apoptotic-like morphological change, which is consistent with a previous study (40). In addition, the time from visible aggregate formation to cell death was markedly similar in the four different mutant PKCγs examined. All SCA14-mutant PKCγs therefore may form amyloid-like aggregates to cause apoptotic cell death. A conversion process from soluble to insoluble aggregates may be highly cytotoxic because diffuse mutant PKCγ-GFP was equally as cytotoxic as diffuse wild-type PKCγ-GFP. This conclusion is also supported by the observation that most cells rapidly died after visible mutant PKCγ aggregates were formed.

In contrast to SH-SY5Y and cultured Purkinje cells, apoptotic cell death has not been observed in Purkinje cells having mutant PKCγ aggregates *in vivo* (24). However, our preliminary EM analysis showed 'dark cell' degeneration in Purkinje cells of mice lentivirally expressing mutant PKCγ but not in Purkinje cells expressing GFP, suggesting that mutant PKCγ aggregates might be toxic to Purkinje cells *in vivo* as well (Supplementary Material, Fig. S6A and B). We have also found abnormal binucleated

10.0 ± 2.7, 14.4 ± 4.5, 19.7 ± 5.0 and 25.3 ± 7.3 (mean ± SD) cells without aggregates of mutant PKCγ (R41P, H101Y, Q127R and F643L, respectively) in each experiment [$^{*}P < 0.05$; $^{**}P < 0.0001$ (inset)]. In individual cells without aggregates, the maximum fluorescent intensity of mutant PKCγ-GFP was measured on the first day after transfection and plotted against their respective survival times. (**G** and **H**) These experiments were performed separately from the experiments described in Figure 6A–F. Therefore, the setting of GFP fluorescent intensity in these experiments was different from that of Figure 6A–F. Neuroblastoma SH-SY5Y cells were transfected with GFP, wild-type PKCγ-GFP or Q127R PKCγ-GFP. One day after transfection, pictures were taken every 15 min and the data were analyzed using MetaMorph software, as described in Materials and Methods. All data were obtained from four independent experiments. We could evaluate 25.3 ± 1.7, 34.8 ± 7.3 and 23.5 ± 4.8 (mean ± SD) cells expressing diffuse GFP, wild-type PKCγ-GFP and Q127R PKCγ-GFP, respectively, in each experiment. (**G**) The mean 10-h survival rate of cells expressing diffuse GFP, wild-type PKCγ-GFP and Q127R PKCγ-GFP. Data are shown as mean ± SEM ($n = 4$). $^{*}P < 0.05$, $^{***}P < 0.001$ (ANOVA, Tukey's test). Diffuse wild-type PKCγ-GFP was equally as cytotoxic as diffuse Q127R PKCγ-GFP (n.s., not significant). These were also more cytotoxic than GFP alone. (**H**) In individual cells without aggregates, the maximum GFP fluorescent intensity was measured on the first day after transfection and plotted against their respective survival times. The survival time of individual cells with diffuse wild-type or Q127R PKCγ-GFP was not correlated with their maximum GFP fluorescent intensity on the first day after transfection (Spearman, not significant).

Purkinje cells expressing mutant PKCγ-GFP but not wild-type PKCγ-GFP *in vivo* (Supplementary Material, Fig. S6C).

Taken together, our findings support the idea that amyloid-like oligomers and fibril formation of mutant PKCγ may contribute to SCA14 pathogenesis like other neurodegenerative diseases and provide amyloid-like fibril formation as a novel potential therapeutic target. It will be interesting to see whether mutant PKCγ amyloid oligomers and fibrils indeed exist and whether they are associated with severe atrophy of the cerebellum observed in SCA14 patients, although SCA14 is a rare and is not a lethal disease, which limits the availability of the post-mortem tissues of the patients.

Potential roles of amyloid-like fibril formation of wild-type PKCγ

We have shown that wild-type PKCγ forms amyloid-like aggregates *in vitro*. We have also found high-MW aggregates of endogenous PKCγ in the total and the Triton-insoluble fractions of the mouse cerebellum. By using cells without transfection, it has long been known that prolonged activation by phorbol ester causes accumulation of PKCs in the detergent-insoluble fraction of cells (6,51,52). More specifically, endogenous PKCγ has been shown to translocate to the detergent-insoluble fraction in response to glutamate in primary hippocampal neurons (53). These previous studies as well as the current one suggest that some fractions of endogenous PKC isoforms might form amyloid-like aggregates in cells under physiological conditions. Until now, this possibility has not been investigated in detail. Amyloid is not always pathological but rather has normal physiological functions (3). PKCs may form amyloid-like aggregates to amplify their local signals in some physiological PKC-dependent pathways, as proposed in several intracellular signaling proteins (54). We anticipate that the current study will promote further research to clarify these issues.

MATERIALS AND METHODS

Plasmid construction

Wild-type and several mutant PKCγ-GFPs or PKCγ-DRms have been described previously (18,43). For GFP-, DRm-, mCherry-, Myc- and FLAG-tagged constructs, full-length human PKCγ, C1A (amino acids 26–89 or 26–100 for pcDNA3.1-Myc), C1B (98–154 or 86–159 for pcDNA3.1-Myc), C2 (156–333) and kinase (318–697) domains were used. They were subcloned into pUC118 (TaKaRa) and then cloned into pcDNA3, pcDNA3.1-Myc, pmCherry-C1 (Clontech) and p3XFLAG-CMV-10 (Sigma). Mutations in each domain were also generated using the QuikChange II XL site-directed mutagenesis kit. All PCR products were verified by sequencing. The molecular size of mutants and domains was verified by immunoblot analysis using anti-PKCγ, anti-GFP, anti-FLAG (M2) and anti-Myc (9E10) antibodies.

Cell culture and transfection

SH-SY5Y, CHO, HeLa and COS-7 cells were maintained in Ham/DMEM containing Glutamax, Ham, MEM and DMEM, respectively. All media were supplemented with 10% fetal bovine serum, 100 units/ml penicillin and 100 μg/ml streptomycin. Transient transfection was performed with Lipofectamine 2000 (Invitrogen) for SH-SY5Y cells or FuGENE^{TM} 6 (Roche) for COS-7, HeLa and CHO cells. Sf9 cells were cultured in EX-CELL^{TM} 420 (JRH Bioscience) containing 10% fetal bovine serum and 0.5% antibiotic/antimycotic (Invitrogen) and maintained in suspension as shaker cultures.

Long-term time-lapse imaging

Long-term time-lapse imaging was performed using a computer-assisted fluorescent microscope, the LCV100 or LCV110 incubation imaging system (Olympus, Tokyo, Japan). This device possesses the ability to monitor fluorescence in living cells under normal culture conditions (37°C, 95% humidity and 5% CO_2). After 1 day of transfection, GFP or mCherry fluorescence of SH-SY5Y cells was observed for 20 or 22 h. Sequential GFP or mCherry fluorescence and DIC images of SH-SY5Y cells were obtained every 15 min and analyzed using MetaMorph software (Molecular Devices Corporation, PA, USA). For Figure 6A–F, the maximum fluorescent intensity of cells with diffuse R41P, H101Y, Q127R, or F643L PKCγ-GFP at 15 min before aggregate formation was 739 ± 144, 773 ± 165, 772 ± 162 or 832 ± 161 (mean ± s.d.), respectively. In order to reduce the effect of the expression level of PKCγ-GFP, we therefore evaluated all cells having diffuse mutant PKCγ-GFP with maximum fluorescent intensity of >700 at the starting point of observation. The experiments for Figure 6G and H were performed separately from those described in Figure 6A–F. Therefore, the setting of GFP fluorescent intensity in these experiments was different from that of Figure 6A–F. To reduce the effect of the expression level of PKCγ-GFP, we evaluated cells with maximum relative GFP fluorescent intensity of 800–1500 at the starting point of observation. Statistical difference in Kaplan–Meier curves was assessed with the log-rank test using GraphPad Prism software.

Synthesis of mutated C1B peptides and *in vitro* [^{3}H]PDBu-binding assay

As mutated C1B peptides are synthesized and purified in the absence of zinc, zinc coordination of these peptides was first carried out as previously reported (35). The PDBu-binding assay was performed by the method described by Sharkey and Blumberg (55), with slight modifications (35). In brief, zinc coordination was carried out in a distilled water solution for each C1 peptide using 5 M equivalent of $ZnCl_2$ at 4°C. After dilution with distilled water, an aliquot of the peptide solution (2.9 μl for 20 nM; 29 μl for 200 nM) was added to the reaction mixture (247.1 μl for 20 nM; 221 μl for 200 nM) consisting of 50 mM Tris–Maleate (pH 7.0–7.4), 10 mg/ml γ-globulin, 50 μg/ml 1,2-dioleoyl-*sn*-glycerol-3-phospho-L-serine and 20 nM [^{3}H]PDBu.

Observation of protein aggregates

DRm- or GFP-tagged mutant PKCγ and DRm- or GFP-tagged domain (C1A, C1B, C2 and KD-GFP) were co-transfected into SH-SY5Y, HeLa and CHO cells. Transfected cells were cultured in glass bottom dishes for 1–2 days until observation. The fluorescence of GFP or DsRed was observed using a Zeiss LSM

510 confocal laser scanning fluorescence microscope at 488 nm of argon laser excitation with a 505/550-nm band-pass barrier filter, or at 543 nm of HeNe laser excitation using a 560-nm long-pass barrier filter, respectively.

Co-immunoprecipitation and immunoblot analysis

COS-7 cells were co-transfected with FLAG-tagged wild-type PKCγ, mutant PKCγ, the C1A, the C1B, the C2 or the kinase domain, and Myc-tagged wild-type PKCγ, mutant PKCγ, the C1A, the C1B, the C2 or the kinase domain. One day after transfection, COS-7 cells were washed once, harvested with ice-cold PBS and resuspended in ice-cold TBS-T (150 mM NaCl, 0.5% Triton X-100 and 50 mM Tris–HCl; pH 7.4) containing 20 μg/ml leupeptin and 1 mM phenylmethylsulfonyl fluoride (PMSF). After homogenization using a sonicator, the cell lysates were cleared by centrifugation for 15 min at 15 000*g* at 4°C. The supernatants were incubated for 2 h at 4°C with anti-Myc (9E10) or anti-FLAG (M2) monoclonal antibodies. Protein complexes were collected with the addition of protein A-sepharose beads (GE Healthcare Bio-Sciences, AB, Uppsala, Sweden) for 1 h at 4°C. Immunoprecipitates were washed at least four times with an ice-cold homogenization buffer or TBS-T and then were added to 2× SDS sample buffer and boiled for 5 min at 95°C. Immunoblot analysis was performed with anti-Myc (9E10) or anti-FLAG (M2) antibody. Quantification of band intensity was performed using Scion image software.

Recombinant protein expression and purification

Recombinant baculoviruses encoding GST-tagged Q127R, V138E or wild-type PKCγ were prepared according to the manufacturer's instruction (Novagen). About 3–4 days after infection, Sf9 cells were collected and washed once with ice-cold PBS and resuspended in ice-cold TBS-T containing 20 μg/ml leupeptin and 1 mM PMSF. After homogenization using a sonicator, the cell lysates were cleared by centrifugation for 15 min at 15 000 *g* at 4°C. The supernatants were incubated for 4 h at 4°C with glutathione–Sepharose 4B resin (GE Healthcare Bio-Sciences). After washing six times with ice-cold TBS-T, the bound proteins were eluted with 50 mM Tris–HCl and 20 mM reduced glutathione at pH 8.0. The recombinant proteins were dialyzed three times against 50 mM Tris–HCl at pH 7.4, 150 mM NaCl, 1 mM EDTA and 1 mM DTT and stored at −80°C until use. In western blot and electron microscopic analyses, 1 mM PMSF and 1 μM leupeptin were added to 50 μl of the protein solution (15–75 μg/ml) during incubation without shaking at 37°C.

Electron microscopy

For purified protein, samples were spread on carbon-coated grids and negatively stained with 1% uranyl acetate and then observed and photographed using a Hitachi 7100 electron microscope (Tokyo, Japan) with an acceleration voltage of 75 kV.

For cultured cells, Ad-CMV-tTA, Ad-TetOp-wild-type PKCγ-GFP and Ad-TetOp-S119P PKCγ-GFP were constructed as previously described (26). The CHO cells were spread on 6-cm (5×10^5 cells/dish) dishes. After 24 h of cultivation, cells were infected with two adenoviral vectors, Ad-CMV-tTA and wild-type or S119P Ad-TedOp PKCγ-GFP, at a multiplicity of infection of 10 and cultured for another 3 days. The cells were washed, harvested and fixed with 5% glutaraldehyde in PBS. After washing out of fixing solution, the cell pellets were re-fixed in 2% osmium tetraoxide in PBS, dehydrated through a graded series of ethanol and then flat-embedded on siliconized slides in Epon. After polymerization at 50°C for 24 h and at 60°C for 24 h, the areas of our interest were cut off and attached to Epon supports for further sectioning on a Reichert-Jung Ultracut E ultramicrotome. Ultrathin sections were mounted on 200-mesh collodion grids (TAAB), stained with 2% uranyl acetate and Reynold's solution and then observed and photographed under a Hitachi 7100 electron microscope.

Thioflavin T fluorescence assay

Sample solution consisting of a recombinant protein, 1 mM PMSF, 1 μM leupeptin and 5 μM thioflavin T was incubated in Sanyo CO_2 incubator model MCO-17A1C (Sanyo Electric Co. Ltd, Osaka, Japan) at 37°C. The sample solution was shaken using a Model 2330 mixer (Wakenyaku Co. Ltd., Kyoto, Japan) during the incubation, and the solution was used for fluorescence measurements. Thioflavin T fluorescence was monitored by Jasco fluorimeter FP (Jasco Co., Tokyo, Japan).

Thioflavin S staining

Two days after transfection, CHO cells expressing mutant PKCγ-DRm were fixed with 4% paraformaldehyde for 30 min at room temperature. Subsequent procedures were performed at room temperature. After washing three times with PBS containing 0.03% Triton X-100 (PBS-T), the cells were treated with PBS containing 0.3% Triton X-100 for 45 min and subsequently stained with 0.001% thioflavin S (Sigma). After washing four times with PBS-T, the cell images were observed with an inverted epi-fluorescence microscope, the Nikon Eclipse TS100F (Nikon Instruments, Tokyo, Japan), equipped with a CCD camera, the Digital Sight DS-2MBVc (Nikon). Filter blocks of G-2A and BV-2A were used for visualizing DRm and thioflavine S, respectively.

Prediction of aggregation-prone regions

The prediction of aggregation-prone regions was performed with the Zyggregator method as previously reported (32).

Brain protein extraction

All animal studies were approved by the Institutional Animal Care and Use Committee and conducted according to the Kobe University Animal Experimentation Regulations. The cerebellums of C57BL/6N male mice were dissected out and homogenized by sonication in ice-cold TBS (50 mM Tris–HCl, 150 mM NaCl, 1 mM EDTA, pH 7.4) containing a protease inhibitor cocktail (Nakalai Tesque). A portion of the homogenate was stored as the total fraction. After centrifugation at 100 000*g* for 30 min at 4°C, the supernatant was stored as the TBS-soluble fraction. The pellet was washed with ice-cold TBS three times and resuspended by sonication to the same volume as the original homogenate in TBS with 1% Triton

X-100 containing a protease inhibitor cocktail. After centrifugation at 100 000*g* for 30 min at 4°C, the supernatant was stored as the Triton-soluble fraction. The pellet was washed and resuspeded by sonication to the same volume in TBS with 2.5% SDS containing a protease inhibitor cocktail and stored as the Triton-insoluble fraction. SDS–PAGE was performed in a non-reducing condition (without mercaptoethanol).

SUPPLEMENTARY MATERIAL

Supplementary Material is available at *HMG* online.

ACKNOWLEDGEMENTS

We thank Dr Toshinobu Suzaki (Kobe University, Kobe, Japan) for help with EM.

Conflict of Interest statement. None declared.

FUNDING

This work was supported in part by a Grant-in-Aid for Scientific Research from the Global Center of Excellence Program of the Ministry of Education, Culture, Sports, Science, and Technology of Japan, a Grant from the Takeda Science Foundation and a Grant-in-Aid from the Japan Society for the Promotion of Science.

REFERENCES

1. Nelson, R. and Eisenberg, D. (2006) Structural models of amyloid-like fibrils. *Adv. Protein Chem.*, **73**, 235–282.
2. Chiti, F. and Dobson, C.M. (2006) Protein misfolding, functional amyloid, and human disease. *Annu. Rev. Biochem.*, **75**, 333–366.
3. Aguzzi, A. and O'Connor, T. (2010) Protein aggregation diseases: pathogenicity and therapeutic perspectives. *Nat. Rev. Drug Discov.*, **9**, 237–248.
4. Eisenberg, D. and Jucker, M. (2012) The amyloid state of proteins in human diseases. *Cell*, **148**, 1188–1203.
5. Knowles, T.P., Vendruscolo, M. and Dobson, C.M. (2014) The amyloid state and its association with protein misfolding diseases. *Nat. Rev. Mol. Cell Biol.*, **15**, 384–396.
6. Newton, A.C. (2003) Regulation by ABC kinase by phosphorylation: protein kinase C as a paradigm. *Biochem. J.*, **370**, 361–371.
7. Pearce, L.R., Komander, D. and Alessi, D.R. (2010) The nuts and bolts of AGC protein kinases. *Nat. Rev. Mol. Cell Biol.*, **11**, 9–22.
8. Saito, N., Kikkawa, U., Nishizuka, Y. and Tanaka, C. (1988) Distribution of protein kinase C-like immunoreactive neurons in rat brain. *J. Neurosci.*, **8**, 369–382.
9. Kose, A., Saito, N., Ito, H., Kikkawa, U., Nishizuka, Y. and Tanaka, C. (1988) Electron microscopic localization of type I protein kinase C in rat Purkinje cells. *J. Neurosci.*, **8**, 4262–4268.
10. Dueñas, A.M., Goold, R. and Giunti, R. (2006) Molecular pathogenesis of spinocerebellar ataxias. *Brain*, **129**, 1357–1370.
11. Soong, B.W. and Paulson, H.L. (2007) Spinocerebellar ataxias: an update. *Curr. Opin. Neurol.*, **20**, 438–446.
12. Colón-González, F. and Kazanietz, M.G. (2006) C1 domains exposed: from diacylglycerol binding to protein-protein interactions. *Biochim. Biophys. Acta.*, **1761**, 827–837.
13. Seki, T., Adachi, N., Abe-Seki, N., Shimahara, T., Takahashi, H., Yamamoto, K., Saito, N. and Sakai, N. (2011) Elucidation of the molecular mechanism and exploration of novel therapeutics for spinocerebellar ataxia caused by mutant protein kinase Cγ. *J. Pharmacol. Sci.*, **116**, 239–247.
14. Koht, J., Stevanin, G., Durr, A., Mundwiller, E., Brice, A. and Tallaksen, C.M. (2012) SCA14 in Norway, two families with autosomal dominant cerebellar ataxia and a novel mutation in the PRKCG gene. *Acta. Neurol. Scand.*, **125**, 116–122.
15. Sailer, A., Scholz, S.W., Gibbs, J.R., Johnson, J.O., Wood, N.W., Plagnol, V., Hummerich, H., Ding, J., Hermandez, D., Hardy, J. *et al.* (2012) Exome sequencing in an SCA14 family demonstrates its utility in diagnosing heterogeneous diseases. *Neurology*, **79**, 127–131.
16. Ganos, C., Zittel, S., Minnerop, M., Schunke, O., Heinbokel, C., Gerloff, C., Zühlke, C., Bauer, P., Klockgether, T., Münchau, A. *et al.* (2013) Clinical and neurophysiological profile of four German families with spinocerebellar ataxia type 14. *Cerebellum*. DOI:10.1007/s12311-013-0522-7.
17. Ueda, T., Seki, T., Katanazaka, K., Sekiguchi, K., Kobayashi, K., Kanda, F. and Toda, T. (2013) A novel mutation in the C2 domain of protein kinase C gamma associated with spinocerebellar ataxia type 14. *J. Neurol.*, **260**, 1664–1666.
18. van Gaalen, J., Vermeer, S., van Veluw, M., van de Warrenburg, B.P. and Dooijes, D. (2013) A de novo SCA14 mutation in an isolated case of late-onset cerebellar ataxia. *Mov. Disord.*, **28**, 1902–1903.
19. Seki, T., Adachi, N., Ono, Y., Mochizuki, H., Hiramoto, K., Amano, T., Matsubayashi, H., Matsumoto, M., Kawakami, H., Saito, N. *et al.* (2005) Mutant protein kinase Cγ found in spinocerebellar ataxia type 14 is susceptible to aggregation and causes cell death. *J. Biol. Chem.*, **280**, 29096–29106.
20. Seki, T., Takahashi, H., Adachi, N., Abe, N., Shimahara, T., Saito, N. and Sakai, N. (2007) Aggregate formation of mutant protein kinase C gamma found in spinocerebellar ataxia type 14 impairs ubiquitin-proteasome system and induces endoplasmic reticulum stress. *Eur. J. Neurosci.*, **26**, 3126–3140.
21. Lin, D. and Takemoto, D.J. (2007) Protection from ataxia-linked apoptosis by gap junction inhibitors. *Biochem. Biophys. Res. Commun.*, **362**, 982–987.
22. Seki, T., Shimahara, T., Yamamoto, K., Abe, N., Amano, T., Adachi, N., Takahashi, H., Kashiwagi, K., Saito, N. and Sakai, N. (2009) Mutant PKCγ found in spinocerebellar ataxia type 14 induces aggregate-independent maldevelopment of dendrites in primary cultured Purkinje cells. *Neurobiol. Dis.*, **33**, 260–273.
23. Asai, H., Hirano, M., Shimada, K., Kiriyama, T., Furiya, Y., Ikeda, M., Iwamoto, T., Mori, T., Nishinaka, K., Konishi, N. *et al.* (2009) Protein kinase Cγ, a protein causative for dominant ataxia, negatively regulates nuclear import of recessive-ataxia-related aprataxin. *Hum. Mol. Genet.*, **18**, 3533–3543.
24. Shuvaev, A.N., Horiuchi, H., Seki, T., Goenawan, H., Irie, T., Iizuka, A., Sakai, N. and Hirai, H. (2011) Mutant PKCγ in spinocerebellar ataxia type 14 disrupts synapse elimination and long-term depression in Purkinje cells *in vivo*. *J. Neurosci.*, **31**, 14324–14334.
25. Kano, M., Hashimoto, K., Chen, C., Abeliovich, A., Aiba, A., Kurihara, H., Watanabe, M., Inoue, Y. and Tonegawa, S. (1995) Impaired synapse elimination during cerebellar development in PKCγ mutant mice. *Cell*, **83**, 1223–1231.
26. Seki, T., Takahashi, H., Yamamoto, K., Ogawa, K., Onji, T., Adachi, N., Tanaka, S., Hide, I., Saito, N. and Sakai, N. (2010) Congo red, an amyloid-inhibiting compound, alleviates various types of cellular dysfunction triggered by mutant protein kinase Cγ that causes spinocerebellar ataxia type 14 (SCA14) by inhibiting oligomerization and aggregation. *J. Pharmacol. Sci.*, **114**, 206–216.
27. Heiser, V., Scherzinger, E., Boeddrich, A., Nordhoff, E., Lurz, R., Schugardt, N., Lehrach, H. and Wanker, E.E. (2000) Inhibition of huntingtin fibrillogenesis by specific antibodies and small molecules: implications for Huntington's disease therapy. *Proc. Natl. Acad. Sci. USA.*, **97**, 6739–6744.
28. Sanchez, I., Mahlke, C. and Yuan, J. (2003) Pivotal role of oligomerization in expanded polyglutamine neurodegenerative disorders. *Nature*, **421**, 373–379.
29. Scherzinger, E., Lurz, R., Turmaine, M., Mangiarini, L., Hollenbach, B., Hasenbank, R., Bates, G.P., Davies, S.W., Lehrach, H. and Wanker, E.E. (1997) Huntingtin-encoded polyglutamine expansions form amyloid-like protein aggregates *in vitro* and *in vivo*. *Cell*, **90**, 549–558.
30. Harper, J.D., Lieber, C.M. and Lansbury, P.T. (1997) Atomic force microscopic imaging of seeded fibril formation and fibril branching by the Alzheimer's disease amyloid-beta protein. *Chem. Biol.*, **4**, 951–959.
31. LeVine, H. 3rd (1999) Quantification of beta-sheet amyloid fibril structures with thioflavin T. *Methods Enzymol.*, **309**, 274–284.
32. Tartaglia, G.G., Pawar, A.P., Campioni, S., Dobson, C.M., Chiti, F. and Vendruscolo, M. (2008) Prediction of aggregation-prone regions in structured proteins. *J. Mol. Biol.*, **380**, 425–436.
33. Glabe, C.G. and Kayed, R. (2006) Common structure and toxic function of amyloid oligomers implies a common mechanism of pathogenesis. *Neurology*, **66**, S74–S78.

34. Haass, C. and Selkoe, D.J. (2007) Soluble protein oligomers in neurodegeneration: lessons from the Alzheimer's amyloid β-peptide. *Nat. Rev. Mol. Cell Biol.*, **8**, 101–112.
35. Shindo, M., Irie, K., Nakahara, A., Ohigashi, H., Konishi, H., Kikkawa, U., Fukuda, H. and Wender, P.A. (2001) Toward the identification of selective modulators of protein kinase C (PKC) isozymes: establishment of a binding assay for PKC isozymes using synthetic C1 peptide receptors and identification of the critical residues involved in the phorbol ester binding. *Bioorg. Med. Chem.*, **9**, 2073–2081.
36. Kazanietz, M.G., Wang, S., Milne, G.W., Lewin, N.E., Liu, H.L. and Blumberg, P.M. (1995) Residues in the second cysteine-rich region of protein kinase Cδ relevant to phorbol ester binding as revealed by site-directed mutagenesis. *J. Biol. Chem.*, **270**, 21852–21859.
37. Stevanin, G., Hahn, V., Lohmann, E., Bouslam, N., Gouttard, M., Soumphonphakdy, C., Welter, M.L., Ollagnon-Roman, E., Lemainque, A., Ruberg, M. *et al.* (2004) Mutation in the catalytic domain of protein kinase Cγ and extension of the phenotype associated with spinocerebellar ataxia type 14. *Arch. Neurol.*, **61**, 1242–1248.
38. Klebe, S., Durr, A., Rentschler, A., Hahn-Barma, V., Abele, M., Bouslam, N., Schöls, L., Jedynak, P., Forlani, S., Denis, E. *et al.* (2005) New mutations in protein kinase Cγ associated with spinocerebellar ataxia type 14. *Ann. Neurol.*, **58**, 720–729.
39. Chen, D.H., Cimino, P.J., Ranum, L.P., Zoghbi, H.Y., Yabe, I., Schut, L., Margolis, R.L., Lipe, H.P., Feleke, A., Matsushima, M. *et al.* (2005) The clinical and genetic spectrum of spinocerebellar ataxia 14. *Neurology*, **64**, 1258–1260.
40. Takemoto, K., Nagai, T., Miyawaki, A. and Miura, M. (2003) Spatio-temporal activation of caspase revealed by indicator that is insensitive to environmental effects. *J. Cell Biol.*, **160**, 235–243.
41. Arrasate, M., Mitra, S., Schweitzer, E.S., Segal, M.R. and Finkbeiner, S. (2004) Inclusion body formation reduces levels of mutant huntingtin and the risk of neuronal death. *Nature*, **431**, 805–810.
42. Leonard, T.A., Rozycki, B., Saidi, L.F., Hummer, G. and Hurley, J.H. (2011) Crystal structure and allosteric activation of protein kinase C βII. *Cell*, **144**, 55–66.
43. Verbeek, D.S., Knight, M.A., Harmison, G.G., Fischbeck, K.H. and Howell, B.W. (2005) Protein kinase C gamma mutations in spinocerebellar ataxia 14 increase kinase activity and alter membrane targeting. *Brain*, **128**, 436–442.
44. Adachi, N., Kobayashi, T., Takahashi, H., Kawasaki, T., Shirai, Y., Ueyama, T., Matsuda, T., Seki, T., Sakai, N. and Saito, N. (2008) Enzymological analysis of mutant protein kinase Cγ causing spinocerebellar ataxia type 14 and dysfunction in Ca^{2+} homeostasis. *J. Biol. Chem.*, **283**, 19854–19863.
45. Verbeek, D.S., Goedhart, J., Bruinsma, L., Sinke, R.J. and Reits, E.A. (2008) PKCγ mutations in spinocerebellar ataxia type 14 affect C1 domain accessibility and kinase activity leading to aberrant MAPK signaling. *J. Cell Sci.*, **121**, 2339–2349.
46. Perander, M., Bjørkøy, G. and Johansen, T. (2001) Nuclear import and export signals enable rapid nucleocytoplasmic shuttling of the atypical protein kinase Cλ. *J. Biol. Chem.*, **276**, 13015–13024.
47. Nelson, R. and Eisenberg, D. (2006) Recent atomic models of amyloid fibril structure. *Curr. Opin. Struct. Biol.*, **16**, 260–265.
48. Tam, S., Spiess, C., Auyeung, W., Joachimiak, L., Chen, B., Poirier, M.A. and Frydman, J. (2009) The Chaperonin TRiC blocks a huntingtin sequence element that promotes the conformational switch to aggregation. *Nat. Struct. Mol. Boil.*, **16**, 1279–1285.
49. Liebman, S.W. and Meredith, S.C. (2010) Sticky N17 speeds huntingtin piles-up. *Nat. Chem. Biol.*, **6**, 7–8.
50. Lansbury, P.T. and Lashuel, H.A. (2006) A century-old debate on protein aggregation and neurodegeneration enters the clinic. *Nature*, **443**, 774–779.
51. Nixon, J.B. and McPhail, L.C. (1999) Protein kinase C (PKC) isoforms translocate to Triton-insoluble fractions in stimulated human neutrophils: correlation of conventional PKC with activation of NADPH oxidase. *J. Immunol.*, **163**, 4574–4582.
52. Gregorio, C.C., Hubo, R.T., Bankert, R.B. and Repasky, E.A. (1992) Translocation of spectrin and protein kinase C to a cytoplasmic aggregate upon lymphocyte activation. *Proc. Natl. Acad. Sci. USA*, **89**, 4947–4951.
53. Buchner, K., Adamec, E., Beermann, M.L. and Nixon, R.A. (1999) Isoform-specific translocation of protein kinase C following glutamate administration in primary hippocampal neurons. *Mol. Brain Res.*, **64**, 222–235.
54. Wu, H. (2013) Higher-order assemblies in a new paradigm of signal transduction. *Cell*, **153**, 287–292.
55. Sharkey, N.A. and Blumberg, P.M. (1985) Highly lipophilic phorbol esters as inhibitors of specific [^{3}H]phorbol 12,13-dibutyrate binding. *Cancer Res.*, **45**, 19–24.